Preparation of 3D Nanoflower-like ZnO/graphene Oxide decorated with Au@AuPt Bimetallic Nanoparticles for Electrochemical Determination of Doxorubicin Hydrochloride

Ling Shi[1], Zefeng Wang[1,2,*], Lae Bai[1], Guangming Yang[1,*]

[1] Engineering Research Center for Processing and Quality Control of Local Characteristic Food and Consumer Goods of High Education in Yunnan Province, College of Science, Honghe University, Mengzi 661199, PR China
[2] Innovation Research Institute of Traditional Chinese Medicine (IRI), Shanghai University of Traditional Chinese Medicine, Shanghai 201203, China
[*]E-mail: wangzefeng841006@163.com, yangguangmingbs@126.com

A novel 3D nanoflower-like ZnO-graphene oxidation (3D ZnO-GO) nanocomposites were proposed for the first time by simple aqueous hydrothermal method and sonochemical approach. Then the Au@AuPt NPs were decorated onto 3D ZnO-GO nanocomposites to obtain a novel Au@AuPt/3D ZnO-GO nanohybrids. The obtained nanohybrids were characterized by scanning electron microscopy, transmission electron microscopy, and X-ray diffraction. The Au@AuPt/3D ZnO-GO nanohybrids were used to fabricate electrochemical sensor for detection of doxorubicin hydrochloride. The proposed sensor showed excellent electrocatalytic activity toward electrochemical oxidation doxorubicin hydrochloride. The electrochemical ocidation reaction of doxorubicin hydrochloride on modified electrode surface was a surface-controlled process, and the charge transfer coefficient (α) and electron transfer number (n) were 0.81 and 2, respectively. The sensor had a wide linear range from 0.65 μM to 369.45 μM, with the limit of detection was 0.013 μM. Furthermore, the proposed electrochemical sensor can be applied successfully to selective determination of doxorubicin hydrochloride in urine sample.

1. INTRODUCTION

Doxorubicin hydrochloride was an important anticancer drug, which had been widely used for the treatment of breast cancer, lymphoma and bladder cancer in clinical treatment [1]. However, the

clinical application of doxorubicin hydrochloride was limited because of some toxic side effects including cardiotoxicity, alopecia, myelosuppression, hypoalbuminemia [2, 3]. Thus, it was necessary to monitor the doxorubicin hydrochloride concentrations in patient's serum or urine to avoid adverse effects and ensure the effectiveness of the treatment and patient safety [4, 5]. Therefore, it was urgently necessary to develop fast, simple, and selective methods for detection of doxorubicin hydrochloride. Electrochemical detection technique had received a dramatic growth in recent years due to wide range application and low cost [6, 7]. As well-known, a great diversity of nanomaterials had been demonstrated exhibiting wonderful properties and can enhance electrochemical performance of proposed sensor.

Recently, Zinc oxide (ZnO) had been thought to be a prominent multifunctional material for electrochemical sensor applications due to its good biocompatibility, nontoxicity, and high chemical stability. The variety of structures of ZnO nanomaterials had been reported, 1D nanorods, needles, and wires, 2D nanoplate, nanosheet, and nanopellets, 3D flower, snowflakes, and coniferous urchin-like. However, pure ZnO usually showed rapid recombination of charge carriers which would limit its application. Graphene oxidation nanosheets exhibited unique performance, such as, excellent chemical stability, high conductivity, and high specific surface area, and would provide an exciting new array of ideas and applications. Based on the above considerations, many researchers had prepared the nanocomposites of reduced graphene oxide with ZnO [8, 9]. Nevertheless, the report about 3D flower-like ZnO-graphene oxidation was relatively few. Meantime, the application of novel Au@AuPt bimetallic nanoparticle decorated flower-like ZnO-graphene oxidation (Au@AuPt/3D ZnO-GO) nanohybrids as high-performance electrocatalysts for constructing a doxorubicin hydrochloride electrochemical sensor had rarely been explored.

In this work, a novel 3D flower-like ZnO was prepared by a simple aqueous hydrothermal method, and then 3D flower-like ZnO-GO nanocomposites were obtained for the first time through a sonochemical approach. Then the Au@AuPt NPs were decorated onto 3D ZnO-GO nanocomposites to obtain a novel nanohybrid. The obtained nanohybrid was used to construct electrochemical senor for doxorubicin hydrochloride.

2. EXPERIMENTAL

2.1. Chemicals

Graphene oxidation was obtained from Jiangsu XFNANO Technology Co., Ltd. Zinc nitrate hexahydrate [$Zn(NO_3)_2 \cdot 6H_2O$], hexamethylenetetramine ($C_6H_{12}N_4$), trisodium citrate dihydrate ($HOC(COONa)(CH_2COONa)_2 \cdot 2H_2O$), anhydrous ethanol, phosphoric acid, glacial acetic acid, boric acid were obtained from Shanghai Chemical Reagent Co. Ltd. (Shanghai, China). Tetrachloroauric (III) acid ($HAuCl_4$), hexachloroplatinic (IV) acid (H_2PtCl_6), doxorubicin hydrochloride were purchased from Shanghai Eybridge Chemical Technology Co., Ltd. A certain amount of doxorubicin hydrochloride was dissolved in Ultra-pure water with ultrasonication for 30 min, and stored in the dark at 4 ◦C. The Britton-Robinson (B-R) buffer solutions (0.04 M in each of acetic, phosphoric and boric

acids) adjust to the desired pH with additions of 0.2 M sodium hydroxide were used as a supporting electrolyte.

2.2. Synthesis of 3D flower-like ZnO and ZnO-GO nanocoposites

0.7437 g $Zn(NO_3)_2 \cdot 6H_2O$ was dissolved in 250 mL ultra-pure water in a round-bottom flask. 0.14 g $C_6H_{12}N_4$ was dissolved in 100 mL ultra-pure water and then added into the above solution under magnetic stirring. 0.0735 g trisodium citrate dehydrate was dissolved in 50 mL ultra-pure water and continued adding to the above solution. The obtained mixed solutions were kept at 95 °C with constant stirring for 2 h. The resultant 3D flower-like ZnO was collected by centrifugation and washed with ultra-pure water and anhydrous ethanol three times. The obtained nanomaterials were marked as ZnO-2.

In order to prepare 3D flower-like ZnO-GO nanocoposites, 10.0 mg GO was dispersed in 10 mL ultra-pure water. The mixture solutions was ultrasonicated for 1 h. Then as-prepared 30 mg 3D ZnO was added into the GO suspension. The obtained solution was subjected to ultrasound (200 W) for 2 h at 50 °C, leading to a light grey solution. The obtained solution was stored at 4 °C for later use.

2.3. Synthesis of Au nanoseeds

Au nanoseeds were prepared according to a modified Frens' method [10]. 1.30 mL 19.302 mM $HAuCl_4$ solution and 48.8 mL ultra-pure water were mixed in three-necked round bottom flask. Then the obtained solution was heated to a boil. Then 0.368 mL 340 mM trisodium citrate solutions were added. The obtained solutions were vigorous stirred and refluxed for 10 min. Finally, the obtained wine red dispersion was stored at 4 °C after cooling.

2.4. Synthesis of Au@AuPt NPs and Au@AuPt/3D ZnO-GO nanohybrids

In a typical method, 2 mL of Au nanoseeds, 1.5 mL of H_2PtCl_4 (1.00 mM) and $HAuCl_4$ (nH_2PtCl_4: $nHAuCl_4$ = 2:1) were mixed in three-necked round bottom flask. The resultant solution was kept at 4 °C under vigorous stirring for 5 min, followed by addition of 0.65 mL $NaBH_4$ (10.00 mM). The mixture was stirred for approximately 30 min. The resulting products were collected by centrifugation and washed with ultra-pure water. Finally, the obtained Au@AuPt NPs were dispersed in 30 mL ultra-pure water. For the syntheses of Au@AuPt/3D ZnO-GO nanohybrids, 30 mL Au@AuPt NPs and 10 mL 3D flower-like ZnO-GO were mixed, then the mixture solutions were ultrasonicated (200 W) for 3 h. the resulting homogeneous dispersion solutions were collected.

2.5. Characterization of the synthesized nano-materials

The morphologies of the as-prepared 3D ZnO and 3D ZnO-GO nanocomposites were observed on a high resolution field emission scanning electron microscopy (SU8010, Hitachi). And the

morphologies of Au@AuPt/3D ZnO-GO nanohybrids were further studied by transmission electron microscope (JEOL 2010, operating at 200 KV). Crystalline properties of the prepared nano-materials were examined using X'Pert[3] powder diffractometer (PANAlytical Company).

2.6. Electrochemical measurements

Before the surface coating, the GC electrode (GCE, 3 mm in diameter) was polished carefully with 1.0, 0.3, and 0.05 μm alumina powder and rinsed with ultra-pure water, followed by sonication in ethanol and ultra-pure water successively. For electrochemical experiments, 7 μL of prepared nanocomposites were dropped on the surface of the GCE and dried in air. The fabricated sensor was used as the working electrode for all electrochemical studies. The electrochemical experiments were performed with a CHI 660E electrochemical analyzer (CH Instruments, Chenhua Co., Shanghai, China). A conventional three-electr ode cell was used, including a Ag/AgCl (saturated KCl) electrode as reference electrode, a platinum wire as counter electrode, and modified GC as working electrode. Electrochemical impedance spectroscopy (EIS) was performed in 1.0 mM $[Fe(CN)_6]^{3-/4-}$ containing 0.1 M KCl as supporting electrolyte within the frequency range of $0.1—10^5$ Hz. The cyclic voltammetry (CV) were carried out in pH=6.0 B-R buffer solution containing 30 μM doxorubicin hydrochloride. The differential pulse voltammetry (DPV) measurments were recorded in the range of 0.2-0.8 V with the applied parameters as follows: amplitude was 0.05 V, pulse width was 0.05 s.

2.7. Analysis of real samples

We used human urine as real samples to determine the doxorubicin hydrochloride content by standard addition method. A certain amount of each real sample was diluted with pH=6.0 B-R buffer solution, spiked with doxorubicin hydrochlorid and then tested to measure doxorubicin hydrochlorid by DPV.

3. RESULT AND DISCUSSION

3.1. Synthesis and characterization of prepared nanomaterials

Flower-like ZnO nanocomposites were prepared under solvothermal condition. $Zn(NO_3)_2•6H_2O$ was used as reactive material, $C_6H_{12}N_4$ was used as uniform precipitant which provided hydroxide ions (OH^-), and trisodium citrate dehydrate used as surface modification agent. In this hydrothermal process, the preparing of flower-like ZnO was endured two-step nucleation growth process. Firstly, $C_6H_{12}N_4$ can provide OH^- according to the equation (1) and (2), the $Zn(NO_3)_2•6H_2O$ provided Zn^{2+}. The $Zn(OH)_2$ can be obtained when $Zn(NO_3)_2•6H_2O$ was mixed with $C_6H_{12}N_4$. Because exist of excess hydroxide ions in the solution, the freshly prepared $Zn(OH)_2$ readily got converted into $[Zn(OH)_4]^{2-}$ (Equ (3)). Then the ZnO crystal nucleus were formed by the dehydration reaction of $[Zn(OH)_4]^{2-}$ (Equ (4)).

$$（CH_2)_6N_4 + 6H_2O \rightarrow 6HCHO + 4NH_3 \qquad \text{Equ (1)}$$

$$NH_3 + H_2O \rightarrow NH_4^+ + OH^- \qquad \text{Equ (2)}$$

$$Zn^{2+} + 2OH^- \rightarrow NH_4^+ + [Zn(OH)_4]^{2+} \qquad \text{Equ (3)}$$

$$[Zn(OH)_4]^{2+} \rightarrow ZnO + H_2O + 2OH^- \qquad \text{Equ (4)}$$
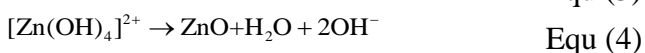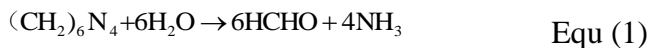
At this stage, a large amount of ZnO crystal nucleus would be produced as the reaction proceeds. The newly formed ZnO nucleus were constantly incorporated into the initial nucleus, and then nanoclusters with certain orientations were formed [11, 12]. The trisodium citrate could reduce surface energy of nanoclusters and regulate nucleation and growth of secondary structures. Then the ZnO nanoclusters grew into a spherical structure and the side length of the ZnO nanosheets increased significantly as the reaction time increased [13]. It was noted that ZnO nanosheets crossed each other and resulting formed a porous network structure. The morphological of ZnO was characterized by scanning electron microscopy (SEM) images. The reaction time was optimized varied from 1 h to 4 h in order to obtain better flower-like structure ZnO. The results were shown in Figure 1 A-H, the obtained ZnO revealed a spherical morphology with diameter ranging from 2 to 3 μm when the reaction time was 1.0 h. And the part of the ZnO surfaces had not formed porous network structure. When the reaction time was increased to 2.0 h, the sheet-like ZnO plates were getting thinner and thinner, the crossover was becoming more obvious resulting a large number of 3D pores structure were formed onto the surface of ZnO structure. Figure 1D revealed the ZnO consisted of numerous nanoflowers, most of nanoflowers were integrated rather than just aggregated with each other. When the reaction time was extended to 3 h, the nanosheets that form the pores structure became rougen and thicken. Finally, at the reaction time of 4 h, the characteristic flower-like structure was disintegrating, and the pores structure was fewer (Figure 1G and 1H). The results proved that the well-defined 3D flower-like ZnO can be obtained when the reaction time was 2 h.

After ultrasound reaction in GO suspension, the surface of 3D flower-like ZnO were coated by thin layers of GO film, the results were shown in Figure 2A. The size of 3D ZnO-GO nanoflowers was about 2.2 μm. It is worth noting that the ZnO still have a 3D flower-like after ultrasound reaction in ZnO-GO nanoflowers. There was no obvious structural changes and collapses, indicating great structural stability. The composite possessed a stable structure due to the introduction of GO nanosheets, which utilizes bend to maintain thermodynamic stability of nanohybrids. Remarkably, the 3D ZnO-GO nanoflowers still possessed a number of pores among petals, which would offer more specific surface area and help not only to load a large number of nanoparticles, but also to increase the contact area between the electrode material and small molecules. It would benefit to accelerate electron transfer during the electrochemical reaction.
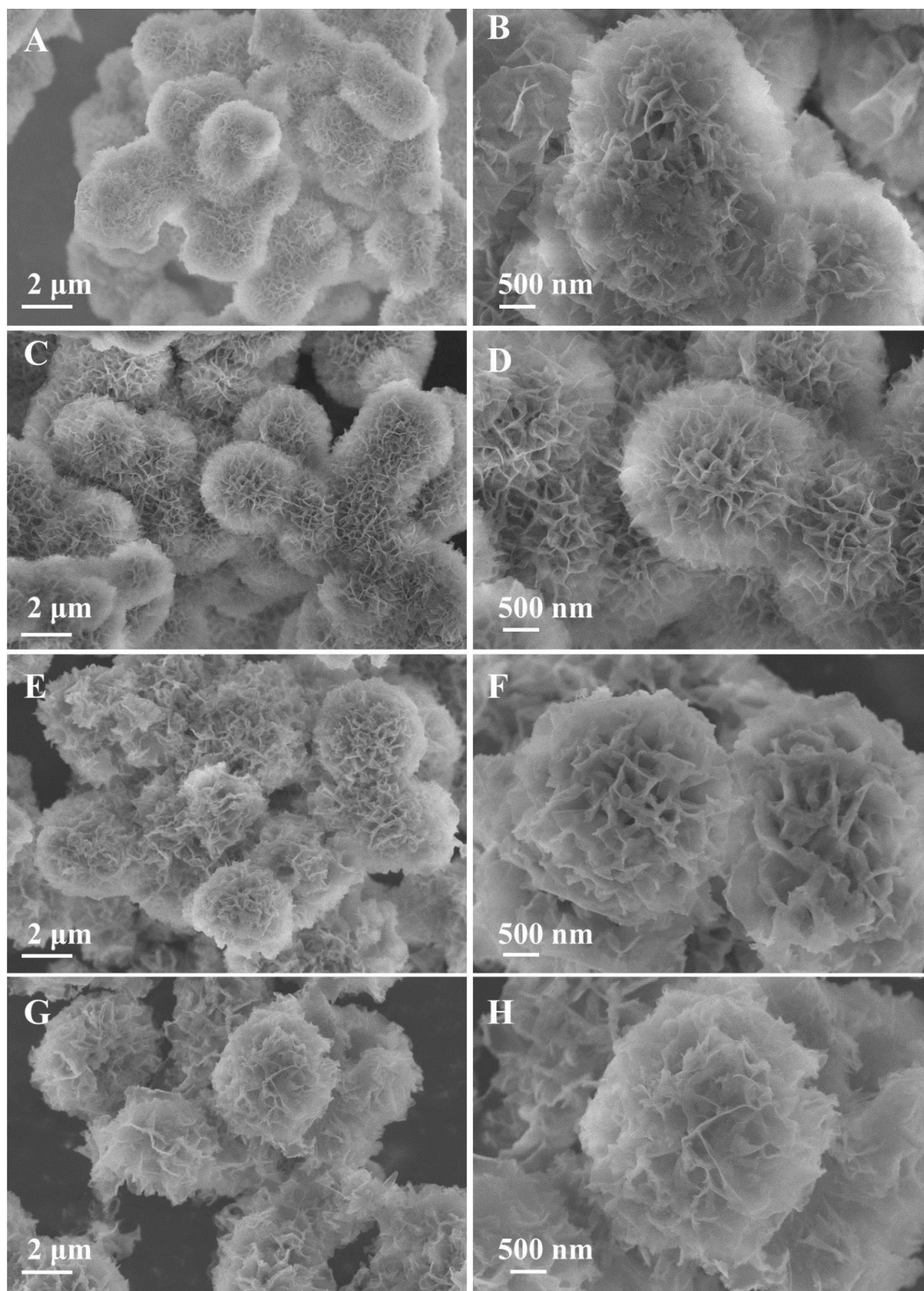
Figure 1. SEM images of 3D ZnO-1 (A and B), 3D ZnO-2 (C and D), 3D ZnO-3 (E and F), and 3D ZnO-4 (G and H), which were obtained with the reaction time of 1 h, 2 h, 3 h, and 4 h, respectively.

The prepared Au nanoseeds and Au@AuPt NPs were characterized by transmission electron microscopy (TEM) images. The results were shown in Figure 2B and C, the results revealed that spherical Au nanoseeds with uniform size were obtained. The size of Au nanoseeds were about 16 nm and there was no obvious agglomeration of Au nanoseeds (Figure 2B). Figure 2C show the TEM images of Au@AuPt NPs, numerous dendritic branches AuPt NPs were grew around of Au nanoseeds. Next, the prepared Au@AuPt NPs were decorated onto the surface of the obtained 3D flower-like ZnO-GO. Figure 2 D and E show the SEM images of prepared Au@AuPt/3D ZnO-GO, it was revealed that Au@AuPt NPs were uniformly distributed on the surface of 3D flower-like ZnO-GO. It can be seen that the introduction of Au@AuPt doesn't radically change the shape of 3D flower-like ZnO-GO. But, there was a significant difference for these two nanomaterials. The Au@AuPt/3D ZnO-GO nanohybrids with the size of ≈3.0 μm were much larger than the 3D ZnO-GO, indicating the Au@AuPt NPs had successfully decorated onto the surface of 3D ZnO-GO nanocomposites. The prepared Au@AuPt/3D ZnO-GO nanohybrids were further characterized by TEM images. The results showed that 3D ZnO-GO nanocomposites showed hierarchical structure of petals (Figure 2F), which could confirm the flower-like 3D ZnO-GO prepared successfully. Furthermore, it was cleared that the Au@AuPt NPs were loaded successfully on the surface of 3D ZnO-GO.
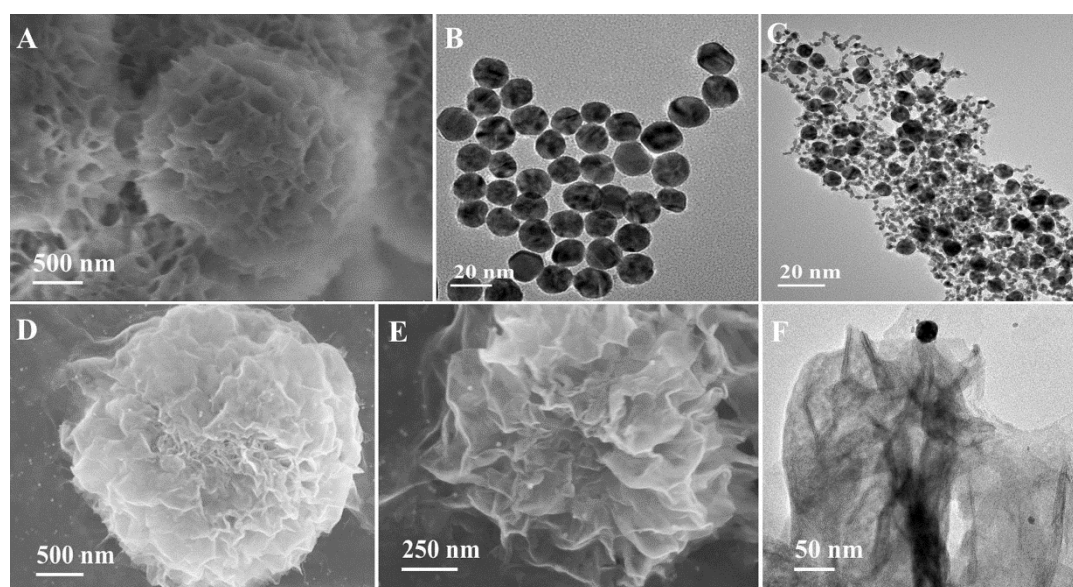
Figure 2. SEM images of 3D ZnO-GO (A), TEM images of Au nanoseeds (A) and Au@AuPt NPs (B), SEM images of Au@AuPt/3D ZnO-GO (D and E), TEM images of Au@AuPt/3D ZnO-GO (F).

The internal lattice of prepared nanomaterials was characterized by XRD analysis. The results were shown in Figure 3. One obvious phase compositions of 3D ZnO (JCPDS 36-1451) can be observed, without other impurity diffraction peaks. The peaks at about 14.32° was observed in all the four materials. It was mainly due to the silicon slice peak and thereby those peaks were neglected in the analysis. XRD diffraction peak of 3D ZnO showed significant characteristic diffraction peaks at 31.84°, 34.62°, 36.40°, 47.65°, 56.75°, 62.95°, and 69.14°, corresponding to the (100), (002), (101),

(102), (110), (103), and (201) plane of 3D ZnO (JCPDS 36-1451) (curve a) [14, 15]. The results clearly indicated that pure 3D ZnO exhibited a hexagonal wurtzite structure with a preferred (101) orientation. In the case of 3D ZnO-GO (curve b), only one significant characteristic diffraction peaks can be observed at about 33.37°, which corresponding to the 002 plane of 3D ZnO. However, no significant characteristic diffraction of GO was observed in the 3D ZnO-GO that maybe due to the very thin GO layer [16]. For reference, Au@AuPt NPs were also measured. The pattern of the Au@AuPt NPs showed several peaks at 38.15°, 43.90°, and 64.62°, arising from the (111), (200), and (220) of Au NPs [17]. And the peaks at 39.92° and 45.02 °were corresponding to the (111) and (200) of Pt NPs [18]. The XRD patterns of Au@AuPt/3D ZnO-GO showed three peaks at 33.11°, 36.27°, and 38.27°. The minute peak shifted of (002) and (101) plane of 3D ZnO from 34.62° to 33.11° and 36.40° to 36.27° with broadening of peak which was due to the interdiffusion of second metal such as Au or Pt that alters the size of 3D ZnO unit cell [19]. The results indicated the formation of the Au@AuPt/3D ZnO-GO nanohybrids.
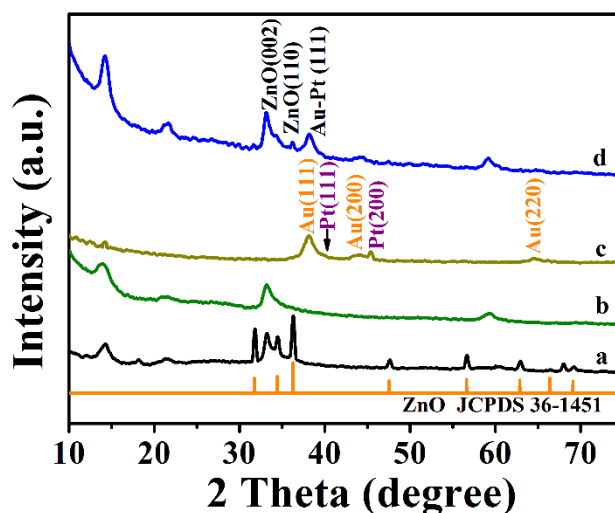
Figure 3. XRD patterns of 3D ZnO (a), 3D ZnO-GO (b), Au@AuPt NPs (c), and Au@AuPt/3D ZnO-GO (d).

3.2. Electrochemical characterization

Cyclic voltammetry (CV) was used to investigate the electrochemical performance of modified electrode using the $[Fe(CN)_6]^{3-/4-}$ as probe molecule. The CVs of GO/GCE, 3D ZnO-GO/GCE, and Au@AuPt/3D ZnO-GO/GCE in 1.0 mM $[Fe(CN)_6]^{3-/4-}$ containing 0.1 M KCl at the scan rate of 100 mV/s were shown in Figure 4A. A pair of redox peak was observed at the GO/GCE, 3D ZnO-GO/GCE, and Au@AuPt/3D ZnO-GO/GCE. The redox peak currents of 3D ZnO-GO/GCE was larger than the GO modified electrode (curve b), which indicated that the 3D ZnO can promote the direct electron transfer between the probe molecule and electrode [20]. For Au@AuPt/3D ZnO-GO/GCE, the peak current was the highest compared with the other two electrodes (curve c). The results proved that Au

NPs and Pt NPs played an important role in the increase of electrochemical activity of prepared Au@AuPt/3D ZnO-GO nanohybrids. Moreover, the highest peak current of Au@AuPt/3D ZnO-GO nanohybrids might be attributed to the large surface area and high conductivity of GO, good electrochemical activity of 3D ZnO, excellent biocompatibility and electrochemical catalytic activity of Au and Pt NPs, and the synergistic effects of Au, Pt, 3D ZnO, and GO in facilitating electron transfer [18, 21, 22]. Furthermore, the EIS technology was a powerful technique to study the electrochemical properties of the electrode surface and can be used to investigate the kinetics of electron transfer at the modified electrode [21, 23, 24]. EIS results of GO/GCE, 3D ZnO-GO/GCE, and Au@AuPt/3D ZnO-GO/GCE were shown in Figure 4B. A well-defined semicircle was observed at GO/GCE (curve a). For the 3D ZnO-GO/GCE, the diameter of the semicircle was significantly reduced (curve b), which indicated that the electron transfer resistance on 3D ZnO-GO/GCE was decreased compared with GO/GCE. The EIS spectra of Au@AuPt/3D ZnO-GO/GCE was almost straight lines (curve c), which revealed that the electron transfer resistance on Au@AuPt/3D ZnO-GO/GCE was greatly decreased compared with the other two electrodes. The EIS results was in good agreement with the CV results, which indicated that the obtained Au@AuPt/3D ZnO-GO nanohybrids had good conductivity and electrochemical activity, and can be beneficial to enhance the electron transfer of target molecular.
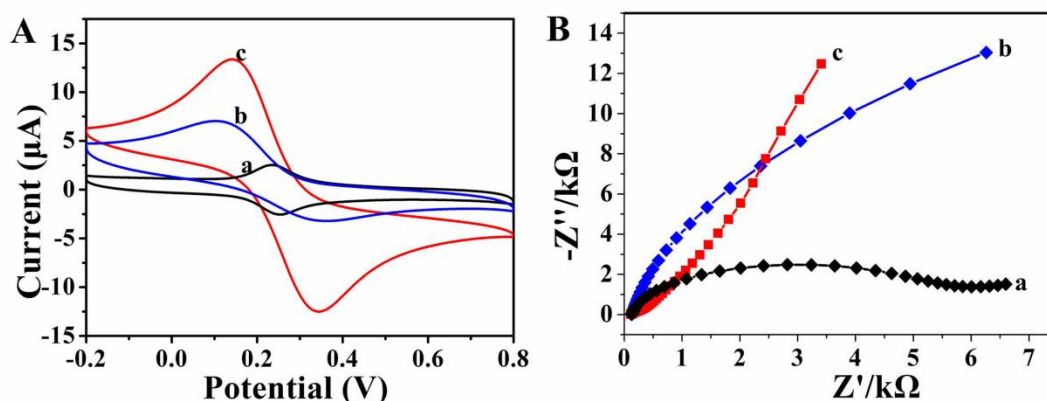
Figure 4. CVs (A) and EIS (B) and of GO/GCE (a), 3D ZnO-GO/GCE (b), and Au@AuPt/3D ZnO-GO/GCE (c) in 1.0 mM $[Fe(CN)_6]^{3-/4-}$ containing 0.1 M KCl at the scan rate of 100 mV/s.

3.3. Electrochemical behavior of doxorubicin hydrochloride on Au@AuPt/3D ZnO-GO/GCE

The electrochemical behavior of doxorubicin hydrochloride at different modified electrodes was investigated by CV pH=6.0 B-R solution. Figure 5A show the responses of Au@AuPt/3D ZnO-GO/GCE in the absence (a) and presence (b) of 30 μM doxorubicin hydrochlorid with a scan rate of 100 mV/s. Not any obvious redox peaks can be observed in the absence of 30 μM doxorubicin hydrochlorid, which indicated that the Au@AuPt/3D ZnO-GO/GCE was electrochemically inactive at 0.3~0.8 V. However, an pair of apparent and reversible redox peaks correspond to the oxidation and reduction of doxorubicin hydrochlorid with the peak potential at 0.57 V and 0.40 V in the presence of

Int. J. Electrochem. Sci., **17** (**2022**) Article Number: 220144

10

30 µM doxorubicin hydrochlorid.

Figure 5B compared the CV response for 30 µM doxorubicin hydrochlorid recorded at GO/GCE (a), 3D ZnO-GO/GCE (b), and Au@AuPt/3D ZnO-GO/GCE (c) in pH=6.0 B-R buffer solution. For the GO/GCE, a weak redox peaks were observed (curve) at 0.55 V and 0.43V, which proved the slower electrochemical reaction of doxorubicin hydrochlorid on GO/GCE surface. When modified with 3D ZnO-GO nanocomposites, a good redox peaks were observed at 0.53 V and 0.41 V. The peak current was larger than the response of GO/GCE toward doxorubicin hydrochlorid. It was maybe due to the 3D ZnO-GO nanocomposites can promote the direct electron transfer between the doxorubicin hydrochlorid and electrode. While Au@AuPt/3D ZnO-GO/GCE exhibited well-defined redox peaks for doxorubicin hydrochlorid. It was noted that the peak current was dramaticlly increased compared with those on the GO/GCE and 3D ZnO-GO/GCE. And the oxidation peak current was 1.6 fold higher than 3D ZnO-GO/GCE. The excellent electrocatalytic activity of Au@AuPt/3D ZnO-GO nanohybrids toward doxorubicin hydrochlorid was mainly attributed to the unique properties of Au@AuPt/3D ZnO-GO nanohybrids. The large specific surface area of GO was benefited for adsorbing doxorubicin hydrochlorid. The excellent electrochemical activity of 3D ZnO, Au and Pt NPs were benefit to enhance electron transfer between electrode and doxorubicin hydrochlorid. These excellent performances of Au@AuPt/3D ZnO-GO nanohybrids leaded to a superb electrocatalytic performances of Au@AuPt/3D ZnO-GO toward doxorubicin hydrochlorid.
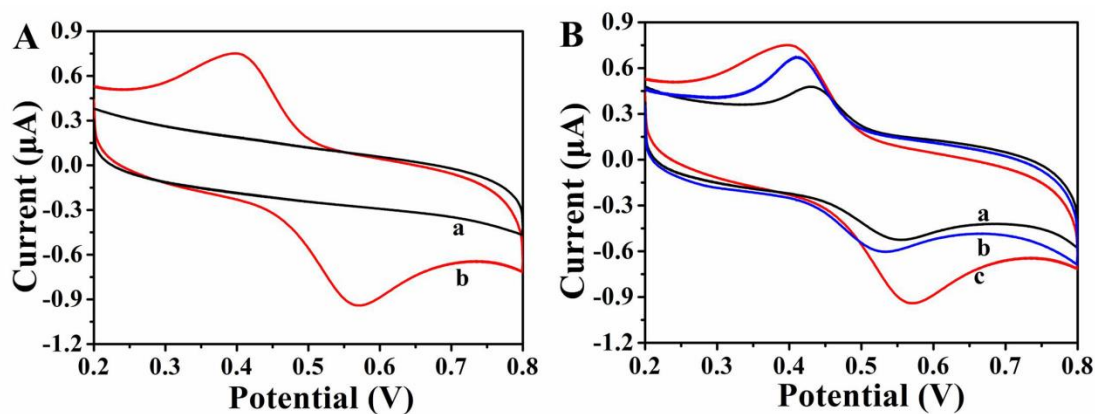
Figure 5. (A) CVs of the Au@AuPt/3D ZnO-GO/GCE in the absence (a) and presence (b) of 30 µM doxorubicin hydrochlorid in pH=6.0 B-R solution with a scan rate of 100 mV/s. (B) CVs of GO/GCE (a), 3D ZnO-GO/GCE (b), and Au@AuPt/3D ZnO-GO/GCE (c) in pH=6.0 B-R solution containing 30 µM of doxorubicin hydrochloride with a scan rate of 100 mV/s.

3.4. Effect of pH

In order to obtain a perfect electrochemical response signal of Au@AuPt/3D ZnO-GO/GCE toward doxorubicin hydrochloride. The pH of buffer solution was optimized using CV at the Au@AuPt/3D ZnO-GO/GCE in B-R solution with different pH values containing 30 µM doxorubicin hydrochlorid at scan rate of 50 mV/s. Figure 6A showed that the redox peak currents were increased

gradually with the increasing pH from 2.45 to 6.0, and then the redox peak currents were reduced when continued to increase the pH to 8.0. A well-defined redox peaks and the maximum redox peaks current were obtained at pH=6 B-R buffer solution. Thus, pH=6 B-R buffer solution was used throughout the experiment. Moreover, it was noticed that the redox peaks potential of doxorubicin hydrochloride was shifted negatively with the increasing of pH, which revealing the participation of H^+ ions in the oxidation reaction. Figure 6B demonstrated the plot between peak potential versus different pH solutions. The linear relationships can be described by the following equations: E_{pa}=-0.069pH+1.04 (R^2=0.9973), E_{pc}=-0.046pH+0.62 (R^2=0.9950), respectively. The slope of calibration curve -0.069 V and -0.046 V were close to the theoretical value -0.059 V, suggesting that the transferred electron number was equal to the number of protons in this electrochemical reaction [22, 25, 26]. The results were in agreement with the literature data [25]. Furthermore, based on the formula [27]: $dE_p/dpH = 2.303mRT/nF$, where n represented the number of electron, m was the number of proton. The m/n can be calculated was 1.17 and 0.78 for the oxidation and reduction processes, respectively. It revealed that the number of electron and proton in the electrochemical reaction of doxorubicin hydrochloride was equal [28]. Therefore, the electrochemical reaction of doxorubicin hydrochloride on the Au@AuPt/3D ZnO-GO/GCE was a two-electron and two-proton process.
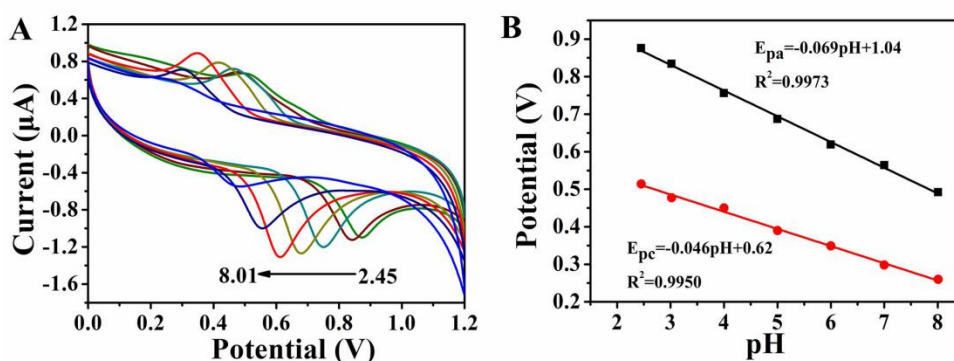
Figure 6. (A) CVs obtained at the Au@AuPt/3D ZnO-GO/GCE in B-R solution with different pH values (2.45, 3.02, 4.0, 5.0, 6.0, 7.0, and 8. 01) containing 30 µM doxorubicin hydrochlorid at scan rate of 50 mV/s. (B) The oxidation and reduction peak potentials of doxorubicin hydrochlorid vs. pH values.

3.5. The oxidation mechanism of doxorubicin hydrochlorid

The oxidation mechanism of doxorubicin hydrochlorid at Au@AuPt/3D ZnO-GO/GCE was investigated by CVs at different scan rates. The CVs of Au@AuPt/3D ZnO-GO/GCE toward 30 µM doxorubicin hydrochlorid at the scan rates from the range of 10-400 mV/s were shown in Figure 7A. Notably, the redox peak currents continuously increased with increasing scan rates. Figure 7B showed that the oxidation and reduction peak currents were linearly proportional to the scan rates. The linear equation was described as: I_{pa}=-0.0103v-0.6231 (R^2=0.9865), I_{pc}=0.0103v+0.1918 (R^2=0.9967), which revealing the oxidation of doxorubicin hydrochlorid was a surface-controlled process [29-31].

Meanwhile, the oxidation peak potential E_{pa} was positively shifted and the reduction peak potential E_{pc} was negatively shift with the scan rate increasing (Figure 7A). Figure 7C revealed that the oxidation and reduction peak potential were linearly proportional to lnv. The equation of linear regression can be described as follows: $E_{pa}=0.0552\ln v+0.391$ ($R^2=0.9964$), $E_{pc}=-0.0133\ln v+0.402$ ($R^2=0.9836$). Based on the Laviron's theory [32], the following equation exists:

$$E_{pa} = E^{0'} + \frac{RT}{(1-\alpha)nF}\ln \upsilon \qquad \text{Eq. (A.1)}$$

$$E_{pc} = E^{0'} - \frac{RT}{\alpha nF}\ln \upsilon \qquad \text{Eq. (A.2)}$$

$$\lg k_S = \alpha\lg(1-\alpha) + (1-\alpha)\lg\alpha - \lg\frac{RT}{nF\upsilon} - \alpha(1-\alpha)\frac{nF\Delta E_p}{2.3RT} \quad \text{Eq. (A.3)}$$

Where E_p was the peak potential, $E^{0'}$ was the formal standard potential, R indicated the universal gas constant ($R=8.314$ J mol^{-1} K^{-1}), T denoted the absolute temperature ($T=298$ K), F was the Faraday's constant ($F=96485$ C mol^{-1}), υ denoted the scan rate, k_s was the electron transfer rate constant, n was electron transfer number. According to the above equation, the value of n, α and k_s can be calculated was 2, 0.81 and 0.38s^{-1}, respectively. These results further confirmed that the electrochemical reaction of doxorubicin hydrochlorid at Au@AuPt/3D ZnO-GO/GCE was two electron transfer process. A possible electrochemical oxidation reaction was proposed as shown in Figure 8. There were electroactive hydroxyl groups on the benzene rings. The oxidation of phenolic hydroxyl of doxorubicin hydrochloride and converted into quinone hydroxyl group [25, 33, 34].
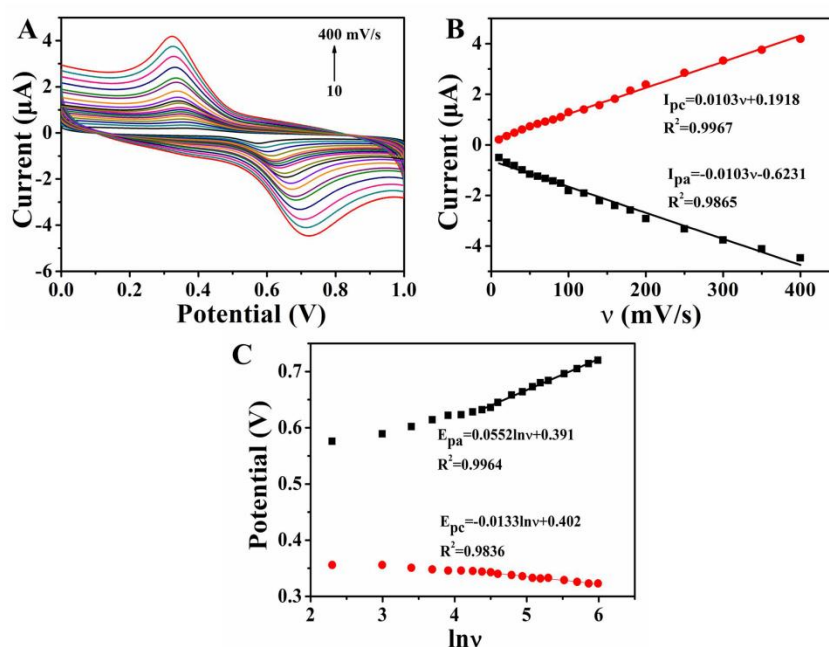
Figure 7. (A) CVs of Au@AuPt/3D ZnO-GO/GCE in pH=6.0 B-R buffer solutions containing 30 μM doxorubicin hydrochlorid at scan rate of 10, 20, 30, 40, 50, 60, 70, 80, 90, 100, 120, 140, 160, 180, 200, 250, 300, 350, and 400 mV/s (from inner to outer curve). (B) Calibration plots of oxidation and reduction peak current vs. scan rates. (C) Plots of oxidation and reduction peak potentials against the lnv.
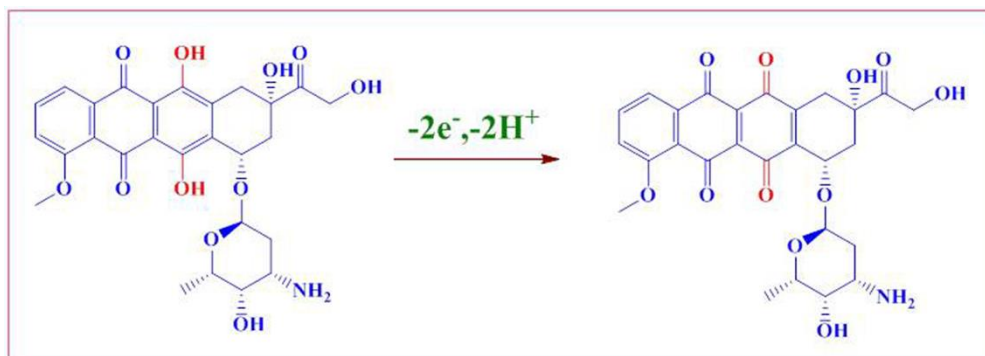
Figure 8. Electrochemical oxidation reaction of doxorubicin hydrochlorid.

3.6. Analytical performance of Au@AuPt/3D ZnO-GO/GCE for doxorubicin hydrochloride detection

The electrochemical performance of Au@AuPt/3D ZnO-GO/GCE toward different concentraction doxorubicin hydrochloride was investigated by DPV in pH=6.0 B-R buffer solutions. The results were shown in Figure 9. The intensity of the oxidation peak current increased with the doxorubicin hydrochloride concentration from 0.65 μM to 369.45 μM. Figure 9B showed the linear dynamic-range plotting of the oxidation peak current (I_{pa}) versus the doxorubicin hydrochloride concentrations over the range of 0.65 μM-369.45 μM, and its linear regression equation can be expressed as I(μA)=-0.0034C(μM)-0.025, R^2=0.9986. The limit of detection for doxorubicin hydrochloride was found to be 0.013 μM.
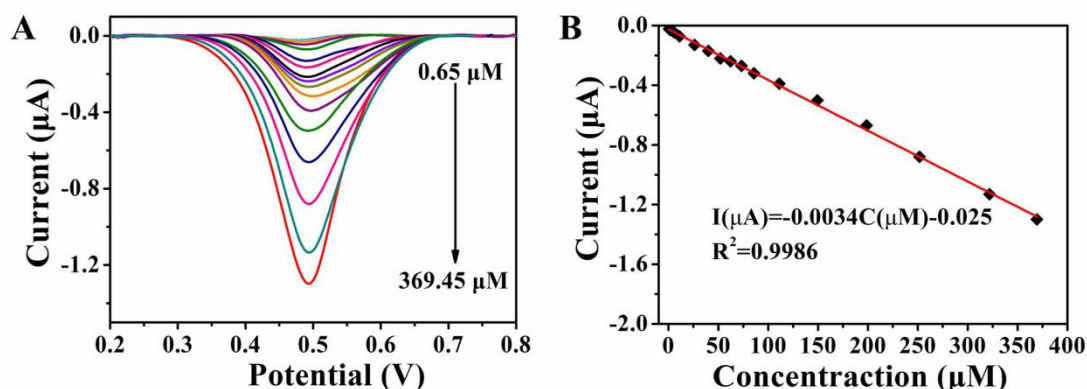
Figure 9. (A) DPV response of Au@AuPt/3D ZnO-GO/GCE in pH=6.0 B-R buffer solutions for different doxorubicin hydrochlorid concentraction: 0.65, 0.96, 2.33, 5.77, 11.01, 26.17, 40.00, 52.08, 62.29, 73.26, 85.79, 111.23, 149.37, 198.64, 251.71, 321.97, and 369.45 μM. (B) The plot of peak current versus concentraction.

3.7. Sability, reproducibility, and interference studies of proposed sensor

The stability of proposed Au@AuPt/3D ZnO-GO/GCE sensor was investigated over a period of 2 weeks. The Au@AuPt/3D ZnO-GO/GCE was used to detect 30 μM doxorubicin hydrochlorid in

pH=6.0 B-R buffer solutions by DPV at a regular interval of 3 days. The results showed that the current responses of doxorubicin hydrochlorid decreased by about 6.3%. The reproducibility of modified electrode was also investigated. Five Au@AuPt/3D ZnO-GO/GCEs fabricated using the same method were used for the determination of 30 μM doxorubicin hydrochlorid in pH=6.0 B-R buffer solutions by DPV. The current obtained from the five independent modified electrodes for doxorubicin hydrochlorid revealed a RSD of 2.27%. Thus, the proposed sensor had excellent reproducibility and stability.

The selectivity of proposed sensor was very important in clinical analytical applications due to various substance were usually existed in biological samples. The proposed sensor was evaluated by detect doxorubicin hydrochlorid in the presence of 100 μM glucose, 100 μM ascorbic acid, 30 μM dopamine, 40 μM uric acid and containing 30 μM doxorubicin hydrochlorid in pH=6.0 B-R buffer solutions. The results indicated that the interfering substance did not affect the detection of doxorubicin hydrochlorid. These results showed that proposed sensor was demonstrated to have good selectivity for doxorubicin hydrochlorid.

3.8. Determination of doxorubicin hydrochlorid in urine sample

In order to evaluate the practicability of proposed sensor. The electrochemical sensor was used to detect doxorubicin hydrochlorid in urine samples by the standard addition method. The results were shown in Table 1, which revealing that the proposed sensor retained its efficiency for the determination of doxorubicin hydrochlorid in urine sample.

Table 1. Determination of doxorubicin hydrochlorid in urine samples (n=3).

sample	added (μM)	Found (μM)^n	Recovery	RSD(%)
1	25.0	26.1	104.4	4.18
2	30.0	29.7	99.0	4.9
3	35.0	34.4	98.3	3.2

4. CONCLUSIONS

A 3D flower-like ZnO-GO nanocomposites were successfully prepared through facile hydrothermal synthesis and ultrasonic methodfor the first time. Then the Au@AuPt NPs were decorated onto 3D ZnO-GO nanocomposites to obtain a novel Au@AuPt/3D ZnO-GO nanohybrids. The morphological and nanostructural characteristics of the prepared Au@AuPt/3D ZnO-GO nanohybrids were characterized by the SEM, TEM, and XRD, confirming the successful preparation of Au@AuPt/3D ZnO-GO nanohybrids. The obtained Au@AuPt/3D ZnO-GO nanohybrids could be an ideal sensing material for recognizing small molecules due to had a number of pores among petals in the obtained nanohybrids. In comparison with GO/GCE and 3D ZnO-GO/GCE, the Au@AuPt/3D

ZnO-GO/GCE exhibited a marked enhancement in the current response, which profit from the higher surface area, porous nature and synergistic effect of the as-prepared hybrid. The results showed that the sensor had a wide linear range from 0.65 μM to 369.45 μM, with the limit of detection was 0.013 μM. The constructed strategy can potentially to extend the application in practical samples.

References

1. I.C. Henderson, D. A. Berry, G. D. Demetri, C. T. Cirrincione, L. J. Goldstein, S. Martino, J. N. Ingle, M. R. Cooper, D. F. Hayes and K. H. Tkaczuk, *J. Clin. Oncol.*, 21 (2003) 976.
2. M. Ali, M. Kamjoo, H. D. Thomas, S. Kyle, I. Pavlovska, M. Babur and B. A. Telfer, *Mol. Cancer Ther.,* 10 (2011) 2320.
3. B. R. Healy-Bird and S. M. Swain, *Clin. Cancer. Res.*, 14 (2008) 14.
4. O. M. Al-Quteimat and M. A. Al-Badaineh, *Saudi Pharm. J. SPJ Off. Publ. Saudi Pharm. Soc.*, 22 (2014) 385.
5. D. D. Von Hoff, M. W. Layard, P. Basa, H. L. Davis, A. L. Von Hoff, M. Rozencweig and F. M. Muggia, *Ann. Intern. Med.*, 91 (1979) 710.
6. L. Shi, Z. F. Wang, N. Wu, X. L. Chen, G. M. Yang and W. Liu, *Int. J. Electrochem. Sci.*, 15 (2020) 3922.
7. L. Shi, Z. F. Wang, N. Wu, G. Z. Gou, X. L. Chen, G. M. Yang and W. Liu, *Int. J. Electrochem. Sci.*, 15 (2020) 3660.
8. G. M. Neelgund and A. Oki, *ACS Omega*, 4 (2019) 5696.
9. W. H. Nam, B. B. Kim, S. G. Seo, L. Y. Soo, J. Y. Kim, W. S. Seo, W. K. Choi, H. H. Park and J. Y. Lee, *Nano Lett.*, 14 (2014) 5104.
10. G. FRENS, *Nat. Phys. Sci.*, 241 (1973) 20.
11. Q. Y. Li, E. B. Wang, S. H. Li, C. L. Wang, C. G. Tian, G. Y. Sun, J. M. Gu and R. Xu, *J. Solid State Chem.*, 182 (2009) 1149.
12. C. Pacholski, A. K. Dipl.-Ing and H. Weller, *Angew. Chem. Int. Ed.,*, 14 (2002) 1188.
13. Y. F. Gao and K. Koumoto, *Cryst. Growth Des.,*, 5 (2005) 1983.
14. H. Gu , Y. Yang , J. X. Tian and G. Y. Shi, *ACS Appl. Mater. Interfaces*, 5 (2013) 6762.
15. P. Roy, A. P. Periasamy, C. T. Liang and H. T. Chang, *Environ. Sci. Technol.*, 47 (2013) 6688.
16. Y. Wang, Z. Li, Y. F. Tian, W. Zhao, X. Q. Liu and J. B. Yang, *J. Mater. Sci.*, 49 (2014) 7991.
17. G. H. Yang, Y. J. Li, R. K. Ranab and J. J. Zhu, *J. Mater. Chem.* A, 1 (2013) 1754.
18. J. D. Qiu, L. Shi, R. P. Liang, G. C. Wang and X. H. Xia, *Chem. Eur. J*, 18 (2012) 7950.
19. P. Gnanaprakasam, J. S. E and T. Selvaraju, *J. Mater. Chem.* A, 3 (2015) 18010.
20. F. Zhang, X. Wang, S. Ai, Z. Sun, Q. Wan, Z. Zhu, Y. Xian, L. Jin and K. Yamamoto, *Anal. Chim. Acta.*, 519 (2004) 155.
21. X. L. Wang, T. Yang, Y. Y. Feng, K. Jiao and G. C. Li, *Electroanalysis*, 21 (2009) 819.
22. Z. F. Wang, G. Z. Gou, L. Shi, J. Yang, C. Xu, L. Zhang, A. P. Fan and Y. Min, *J. Appl. Polym. Sci.*, (2018) 46720.
23. A. Benvidi, N. Rajabzadeh, M. Mazloum-Ardakani, M. M. Heidari and A. Mulchandani, *Biosens.*

Int. J. Electrochem. Sci., 17 **(2022)** Article Number: 220144

16

Bioelectron., 58 (2014) 145.

24. Q. W. Lian, Z. F. He, Q. He, A. Luo, K. W. Yan, D. X. Zhang, X. Q. Lu and X. B. Zhou, *Anal. Chim. Acta*, 823 (2014) 32.
25. A. Shams and A. Yari, *Sensor. Actuator. B Chem.*, 286 (2019) 131.
26. S. Kurbanoglu, B. Bozal-Palabiyik, M. Gumustas, B. Uslu and S. A. Ozkan, *Rev. Roum. Chim.*, 60 (2015) 491.
27. E. Laviron, *J. Electroanal. Chem.*, 52 (1974) 355.
28. J. L. Wang, J. E. Huo, J. Li, E. B. Shang guan and Q. M. Li, *Anal. Methods*, 5 (2013) 4119.
29. L. Shi, Z. F. Wang, N. Wu, X. L. Chen, G. M. Yang and W. Liu, *Int. J. Electrochem. Sci.,*, 15 (2020) 3204
30. X. Zhang, K. P. Wang, L. N. Zhang, Y. C. Zhang and L. Shen, *Anal. Chim. Acta*, 1036 (2018) 26.
31. D. B. Lu, Y. Zhang, L. T. Wang, S. X. Lin, C. M. Wang and X. F. Chen, *Talanta*, 88 (2012) 181.
32. K. Sheng, L. Wang, H. C. Li, L. Zou and B. X. Ye, *Talanta,* 164 (2017) 249.
33. M. Abbasghorbani, *J. Mol. Liq*., 266 (2018) 176.
34. E. Arkan, G. Paimard and K. Moradi, *J. Electroanal. Chem*., 801 (2017) 480.